Applied Catalysis B: Environmental 158–159 (2014) 202–208

Contents lists available at ScienceDirect

Applied Catalysis B: Environmental

journal homepage: www.elsevier.com/locate/apcatb

High-temperature calcination and hydrogen reduction of rutile TiO_2: A method to improve the photocatalytic activity for water oxidation

Fumiaki Amano*, Masashi Nakata

Graduate School of Environmental Engineering, The University of Kitakyushu, 1-1 Hibikino, Wakamatsu-ku, Kitakyushu, Fukuoka 808-0135, Japan

ARTICLE INFO

Article history:
Received 25 January 2014
Received in revised form 9 April 2014
Accepted 13 April 2014
Available online 22 April 2014

Keywords:
Defect chemistry
Hydrogenation
Oxygen vacancy
Structure–activity relationships
Titanium dioxide

ABSTRACT

Rutile titania (TiO_2) is an efficient photocatalyst for oxidizing water to O_2. The photocatalytic activity of particulate rutile for water oxidation was significantly improved by H_2 reduction at 700 °C, after calcination at 1100 °C. The improved activity was due to an increase in crystalline size during calcination, and an increase in conduction band electron concentration by the creation of oxygen vacancies. In contrast to the consideration that oxygen vacancy increases the recombination of electron and holes, the hydrogenated TiO_2 exhibited high apparent quantum efficiency for O_2 evolution, 41% under irradiation at 365 nm. It was found that H_2 treatment improved the photocatalytic activity per unit of surface area not only for O_2 evolution but also for H_2 evolution and acetic acid decomposition. The effect of H_2 reduction treatment was obtained only if the rutile particle was previously calcined at temperatures higher than 1000 °C. This suggests that space charge layer in large crystalline particles is involved in the activation mechanism of hydrogenated rutile TiO_2 particles.

1. Introduction

Solar water-splitting on oxide photocatalysts and semiconductor electrodes is attractive, because of its potential for H_2 production using renewable energy [1–5]. A significant enhancement of the photocatalytic activity for solar energy conversion to chemical fuels is necessary for practical use. However, the design concepts of optimized efficiency photocatalysts have not been clear, even for the typical n-type oxide photocatalyst TiO_2. Rutile TiO_2 particles reportedly achieved photocatalytic splitting of pure water into H_2 and O_2, but the quantum efficiency was estimated to be low, about 1% at 350 nm [6].

Decreasing the density of crystal defects is generally considered to increase the utilization of photoexcited electrons and holes. This is because defects act as recombination centers. Crystal defects in non-doped n-type TiO_2 are considered to be O vacancies and Ti^{3+}. Strong oxidation at elevated temperatures can reportedly decrease the density of defects in TiO_2 [7,8]. Therefore, high-temperature annealing in air is likely to improve the photocatalytic activity.

O vacancies form also shallow donor states below conduction band originating from Ti 3d orbitals, which can even overlap the conduction band in the case of highly deficient TiO_2 [9]. The increase of the concentration of electrons enhance the electrical conductivity of TiO_2 [7]. Actually, single crystal rutile electrodes are often treated by H_2 reduction, to generate O vacancies and improve their electrical conductivity and photoelectrochemical efficiency [10–12].

H_2 reduction treatment has received much recent attention, for improving the photoactivity of anatase TiO_2 nanostructures [13–18]. It works by creating defect disorders on the surface. However, the O vacancy of anatase TiO_2 is considered to be unstable in air even at room temperature, and the enhanced photocatalytic activities of hydrogenated TiO_2 are open for discussion [19,20]. Most investigations have focused on hydrogenated anatase rather than rutile TiO_2. There are few reports on H_2 reduction treatment on particulate rutile photocatalysts, despite rutile being an important photocatalyst for water splitting.

We recently reported that high-temperature calcination deactivated the photocatalytic activity of rutile TiO_2 particles with small specific surface area (2.3 $m^2 g^{-1}$). Subsequent H_2 reduction treatment then improved the activity of the same sample [21]. The surface area was constant during calcination, so deactivation was not attributed to specific surface area changes. Deactivation was partly attributed to a decrease in long-lived photoexcited carriers, accompanied with a decrease in O vacancies through the high-temperature calcination.

Crystalline size is another factor affecting the lifetime of photogenerated charge carriers in photocatalysts. In the photocatalytic O_2 evolution by water oxidation, anatase particles exhibit poor activity, while larger rutile particles are more efficient

* Corresponding author. Tel.: +81 93 695 3372.
E-mail address: amano@kitakyu-u.ac.jp (F. Amano).

http://dx.doi.org/10.1016/j.apcatb.2014.04.025
0926-3373/

[22–24]. Large tungsten trioxide (WO_3) particles with low surface area-to-volume ratios are well-suited to providing long-lived photogenerated holes. This is because slow bulk recombination is the dominant process in larger particles, rather than fast surface recombination [25].

Controlling the crystalline size and O vacancy density is expected to improve the activity of particulate photocatalysts, for O_2 evolution by water splitting. In the current study, we investigated the effect of crystal growth and defect density on the photocatalytic activity of large specific surface area ($17\,m^2\,g^{-1}$) rutile particles. High-temperature calcination and H_2 reduction effectively improved the surface reactivity of rutile photocatalysts. We have found that the effect of H_2 reduction is obtained only for rutile particles with large crystalline size after high temperature calcination.

2. Experimental

2.1. Materials

High purity TiO_2 powder, F-1R (0.02 wt.% Cl), was sourced from Showa Titanium (Toyama, Japan). The powder in an alumina crucible was calcined at 300–1250 °C for 2 h in air, using an electric furnace. After calcination at high temperature, the sample was lightly ground in an alumina mortar. H_2 reduction of the rutile powder was performed in a quartz tube reactor under atmospheric pressure. The sample in a quartz boat was placed in the reactor. The temperature was increased to 700 °C, under a stream of $50\,mL\,min^{-1}$ H_2. After 2 h under the H_2 flow, the sample was cooled to 300 °C under H_2 flow, and then to room temperature under N_2 flow. The sample name F*x*00-H700 indicates that F-1R was calcined at *x*00 °C, followed by H_2 reduction at 700 °C.

2.2. Photocatalytic activity tests

Photocatalytic activity was examined using three test reactions: (A) O_2 evolution with the deposition of Ag^0 on the photocatalyst surface, from aqueous $50\,mmol\,L^{-1}$ $AgNO_3$ (>99.8%, Wako Pure Chemical Industries, Osaka, Japan) under Ar; (B) H_2 evolution from aqueous 50 vol.% ethanol with hexachloroplatinic acid ($H_2[PtCl_6]{\cdot}6H_2O$, >98.5%, Kanto Chemical, Tokyo, Japan) for in situ Pt deposition (2.0 wt.%); (C) oxidative decomposition of 1.0 vol.% aqueous acetic acid under O_2. The 50 mg TiO_2 powder suspension in 9.0 mL of solution in a glass tube with an outside diameter of 18 mm was magnetically stirred, and irradiated by UV emitting diodes (LEDs) at room temperature. The LED wavelength was centered at 380 nm, with a half width of 12 nm. The irradiance was measured to be about $10\,mW\,cm^{-2}$. The amount of evolved gas was quantified by gas chromatography, with a Molecular Sieve-5A column and Porapak-Q column.

Quantum efficiency was measured using monochromatic light through a bandpass filter (central wavelength 365 nm, half bandwidth 10 nm) emitted from a 300 W Xe lamp (ILC Technology CERMAX-LX300). The intensity of irradiation was measured by an optical power meter (Hioki 3664). The apparent (or external) quantum efficiency (AQY) was calculated as the ratio of the rate of electron consumption, assuming that O_2 evolution is a $4e^-$ process, to the flux of incident photons ($\sim 1.7 \times 10^{-6}$ einsteins min^{-1}).

2.3. Characterization

Scanning electron microscopy (SEM) images were recorded using a Hitachi S-5200 instrument. Specific surface areas were determined using Brunauer–Emmett–Teller (BET) plots from N_2 absorption isotherms at −196 °C, measured with a Bel Japan BELSORP-mini instrument. X-ray diffraction (XRD) patterns were recorded on a Rigaku RINT-2000/PC diffractometer, with Cu Kα radiation. Nickel oxide was used as an internal standard. The weight fraction of rutile phase in the anatase-rutile mixture (X_R) was estimated from:

$$X_R = \frac{1.26 I_R}{(I_A + 1.26 I_R)}$$

where I_R and I_A are the intensities of the rutile(1 1 0) and anatase(1 0 1) peaks, respectively [26]. The diameter of rutile crystalline domains was estimated from the half width of rutile(1 1 0) peaks, using the Scherrer equation. Diffuse reflectance ultraviolet–visible–near infrared (UV–Vis–NIR) spectra were obtained using an ALS SEC2000 spectrometer, with a Hamamatsu Photonics L10290 fiber light source and barium sulfate reference.

3. Results

3.1. Characterization of rutile TiO_2 particles

Commercial TiO_2 (F-1R, Showa Titanium) was used as a photocatalyst. Fig. 1 shows SEM images of F-1R and samples calcined at different temperatures for 2 h. Samples calcined at *x*00 °C are denoted as F*x*00. The particle size gradually increased with increasing calcination temperature. After calcination at 1100 °C, the particle size had increased to ~1 μm. This crystal growth caused the specific surface area of F-1R ($17\,m^2\,g^{-1}$) to consistently decrease, with increasing calcination temperatures at >700 °C as shown in Fig. 2. The specific surface area of F1100 was $1.6\,m^2\,g^{-1}$.

XRD patterns indicate that F-1R possessed a rutile TiO_2 phase, with a small fraction of anatase (Fig. A.1 in Appendix A. Supplementary data). The weight fraction of rutile F-1R was ~96%. XRD peaks assigned to anatase disappeared after calcination at 900 °C. The diameter of crystalline domains was estimated by the Scherrer equation, and consistently increased with increasing calcination temperature at >700 °C (Fig. A.2). The crystal growth resulted in an increased particle size and decreased specific surface area.

Fig. 3 shows diffuse reflectance UV–Vis–NIR spectra. The photoabsorption edges due to transition from the valence to conduction bands occurred at approximately 420 nm. This corresponded to the 2.95 eV band gap of rutile TiO_2. There was a difference in the baseline intensity at 420–1050 nm in the spectra. The NIR intensity gradually decreased with increasing calcination temperature. The broad NIR absorption was assigned to the excitation of conduction band electrons, and therefore reflected the carrier concentration in the conduction band [27]. The decrease in intensity upon high-temperature calcination suggested a decreased conduction band electron concentration with crystal growth. This might be related to the decrease of defects upon high-temperature calcination. Strong oxidation reportedly facilitates the transformation of O-deficient to stoichiometric TiO_2 and then metal-deficient TiO_2, with p-type properties [7,8].

3.2. Hydrogen reduction of rutile TiO_2

H_2 reduction treatment of the calcined samples was then carried out. Hydrogenation creates surface O vacancies, and is accompanied by the formation of Ti^{3+} species according to Scheme 1. The optimum H_2 reduction temperature was 700 °C. Samples treated with H_2 at 700 °C for 2 h are denoted as F*x*00-H700. F1100-H700 was a pale blue color, which remained stable in air at room temperature for in excess of one year. The diffuse reflectance spectra show an intense UV absorption assigned to interband transition, and a broad visible–NIR absorption (Fig. 3). The blue coloration and broad visible-NIR absorption were explained by the presence of conduction electrons associated with the generation of O vacancies and Ti^{3+} species [27]. The intensity of the broad visible-NIR absorption

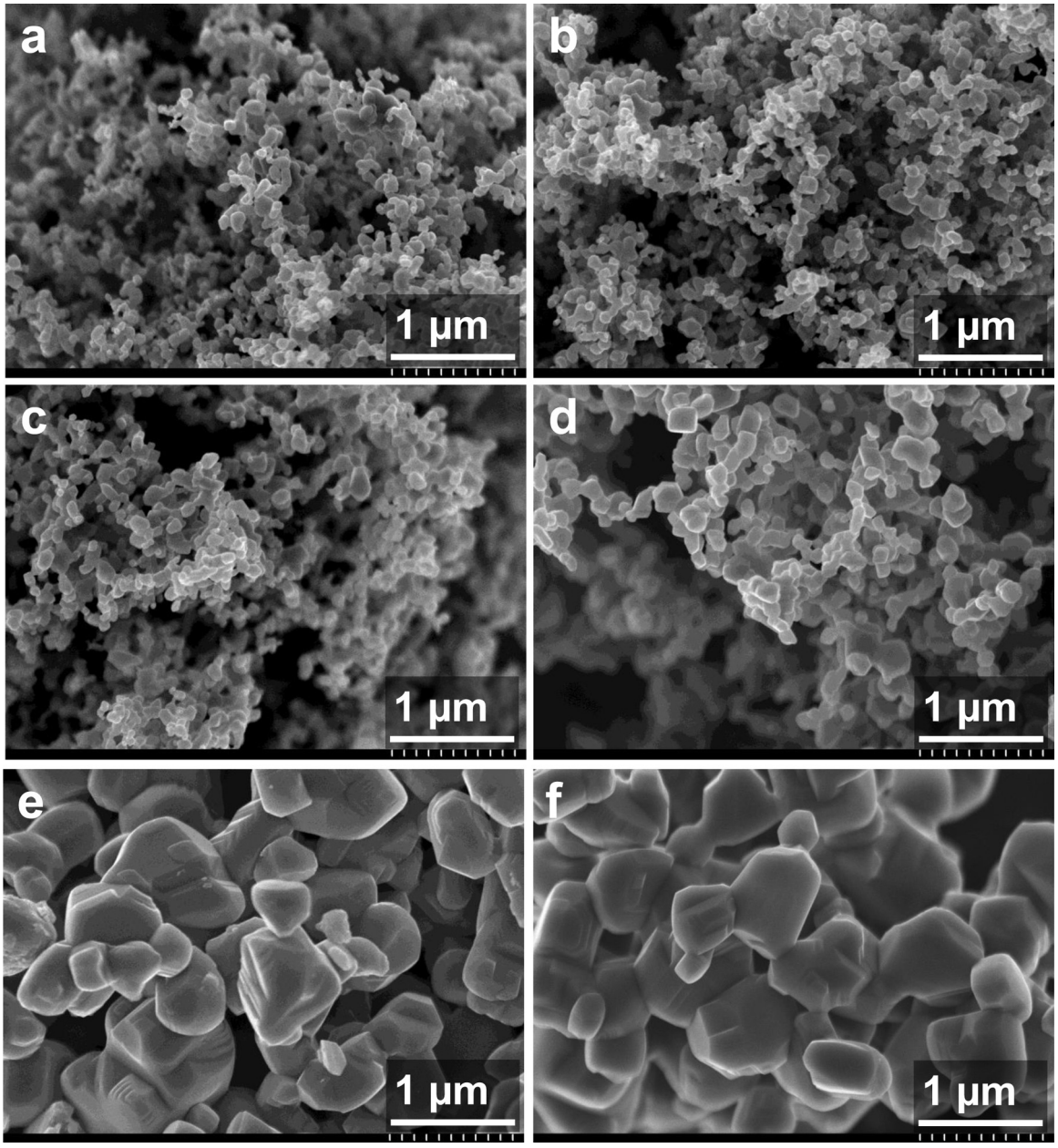

Fig. 1. SEM images of (a) F-1R, (b) F500, (c) F700, (d) F900, (e) F1100, and (f) F1100-H700.

in F1100-H700 was higher than that in F700-H700 and F900-H700. This indicated that the electron concentration in F1100-H700 was higher than that in H_2-treated samples after calcination, at temperatures <1100 °C. The morphology, specific surface area, XRD pattern profile, and crystalline sizes showed little change upon H_2 treatment (Figs. 1 and 2, A.1, and A.2).

3.3. Photocatalytic activity for water oxidation

Photocatalytic activities were tested using three reactions under UV irradiation. Fig. 4 shows the effect of calcination temperature on the rate of reaction (A): photocatalytic O_2 evolution with silver deposition ($4Ag^+ + 2H_2O \rightarrow 4Ag^0 + O_2 + 4H^+$). The rate of photocatalytic O_2 evolution ($r(O_2)$) was evaluated from the amount of O_2 evolved during the period from 20 to 80 min of irradiation (Fig. A.3). Calcination at 1100 °C increased $r(O_2)$ of the pristine sample by 1.9 times. $r(O_2)$ decreased upon calcination at temperatures >1100 °C. When samples were treated with H_2 at 700 °C, $r(O_2)$ increased, especially for those previously calcined at >1000 °C. F1100-H700 was calcined at 1100 °C and followed by H_2 reduction at 700 °C, and exhibited the highest $r(O_2)$, which was 3.6 times that of pristine F-1R. The AQY for O_2 evolution was calculated to be 8.3 and 41% for pristine F-1R and F1100-H700, respectively, under irradiation at 365 nm. The AQY of F1100-H700 was 4.9 times higher than that of pristine F-1R under these conditions. The AQY was comparable to that of TiO_2 (51% at 365 nm) [28] and higher than that of Cs-modified WO_3 (25% at 365 nm) [29] for O_2 evolution in the presence of Fe^{3+}.

$r(O_2)$ over F1100-H700 was constant until complete depletion of Ag^+ (450 μmol), indicating the stability of the hydrogenated TiO_2 photocatalysts. This constant rate is in contrast to results reported for other photocatalysts, in which $r(O_2)$ typically decreased with reaction time. This decrease was because of the decreased Ag^+ concentration, increased pH, and light shielding by Ag^0 deposited on the photocatalyst surface [30]. It should be noted that O vacancies in rutile TiO_2 is stable during photocatalytic condition, since the spent

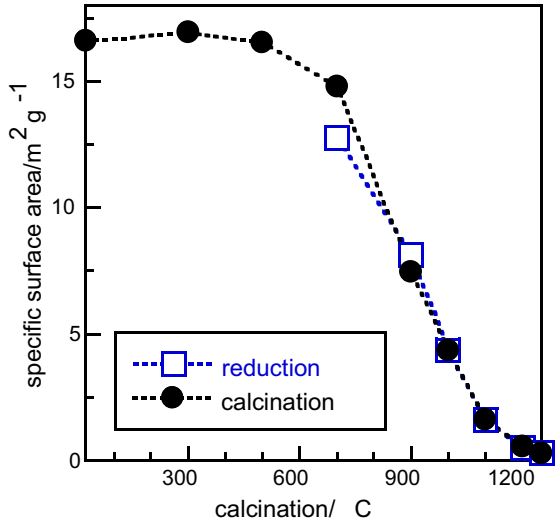

Fig. 2. Specific surface areas of samples treated by (circles) calcination at different temperatures, and (squares) subsequent reduction with H_2 at 700 °C.

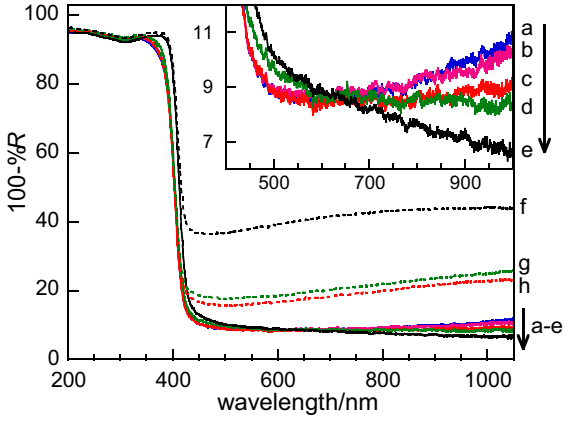

Fig. 3. Diffuse reflectance UV–Vis–NIR spectra of (a) F-1R, (b) F500, (c) F700, (d) F900, (e) F1100, (f) F1100-H700, (g) F900-H700 and (h) F700-H700. (For interpretation of the references to colour in the text, the reader is referred to the web version of this article.)

$$O_O^{2-} + 2Ti^{4+} + H_2 \rightarrow V_O + 2Ti^{3+} + H_2O$$

Scheme 1. H_2 reduction of TiO_2 to produce O-deficient TiO_{2-x}, where V_O represents O vacancies.

photocatalysts were possible to be used repetitively (Fig. A.4). The evolved O_2 was found to reach 225 μmol, which corresponds to the consumption of 900 μmol of Ag^+, over the hydrogenated TiO_2 (626 μmol) after two photocatalytic cycles.

3.4. Photocatalytic efficiencies per unit of surface area

Specific surface area generally affects the photocatalytic activity. Photocatalytic efficiencies per unit of surface area were calculated, to compare surface reactivities. Fig. 5 shows the surface $r(O_2)$, defined as $r(O_2)$ per unit of surface area. The surface $r(O_2)$ of calcined samples consistently increased, with increasing calcination temperature. The surface reactivity for O_2 evolution by samples previously calcined at >1000 °C was significantly improved by H_2 reduction. Fig. 6 shows the rate of H_2 evolution ($r(H_2)$) normalized to surface area, for reaction (B): H_2 evolution from aqueous ethanol solution with in situ deposited Pt co-catalyst. Fig. 7 shows the rate of CO_2 evolution ($r(CO_2)$) normalized to surface area, for

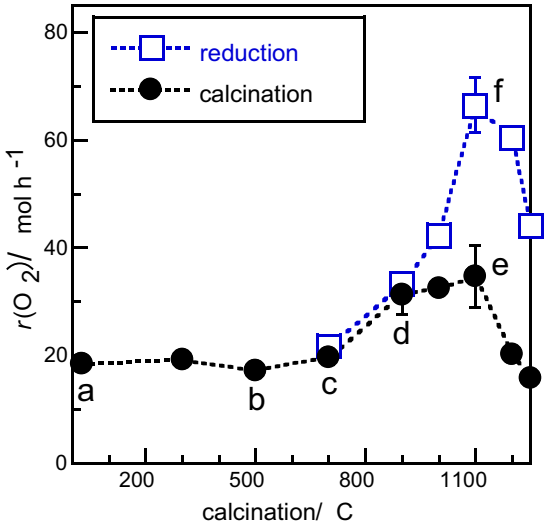

Fig. 4. Rate of photocatalytic O_2 evolution ($r(O_2)$) from water oxidation in the presence of sacrificial $AgNO_3$, over F-1R samples treated by (circles) calcination at different temperatures, and (squares) subsequent reduction with H_2 at 700 °C. Samples (a–f) are the same as those in Fig. 1.

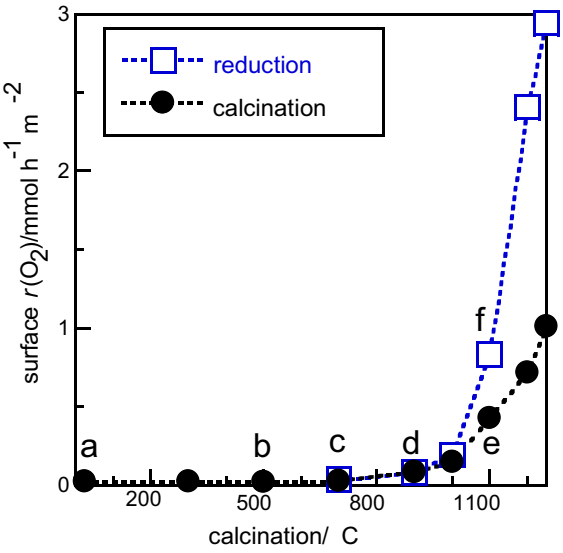

Fig. 5. $r(O_2)$ per unit of surface area over F-1R samples treated by (circles) calcination at different temperatures, and (squares) subsequent reduction with H_2 at 700 °C. The data are reproduced from Fig. 4.

reaction (C): CO_2 evolution by oxidative decomposition of aqueous acetic acid. The rates of H_2 and CO_2 evolution were evaluated from the amount of gas evolved during the period from 20 to 120 min of irradiation (Figs. A.5 and A.6). For reactions (B) and (C), the rate per unit of surface area gradually increased with increasing calcination temperature, but decreased at >1000 °C. The surface rate was enhanced by H_2 reduction treatment for each reaction. The enhancement was more significant for samples previously calcined at high temperatures. H_2 reduction effectively improved the surface reactivity, without being specific to a particular photocatalytic reaction. Thus, the improvement was not due to the creation of catalytic active sites for water oxidation, although O vacancies reportedly act as active sites for water dissociation in rutile(1 1 0) TiO_2 [31]. In reactions (B) and (C), the actual photocatalytic efficiency per light irradiation area gradually decreased with increasing calcination temperature, as a result of the decreased specific surface area (Fig. A.7). This is in spite of the increase in efficiency per unit of surface

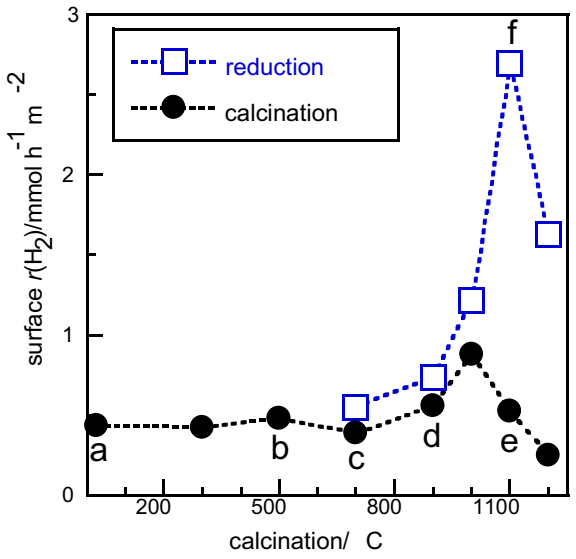

Fig. 6. $r(H_2)$ from aqueous 50 vol.% ethanol solution per unit of surface area over F-1R samples treated by (circles) calcination at different temperatures, and (squares) subsequent reduction with H_2 at 700 °C. Samples (a–f) are the same as those in Fig. 1.

area. Therefore, actual photocatalytic efficiency per light irradiation area was enhanced only for water oxidation by the treatment of high-temperature calcination and hydrogenation.

4. Discussion

4.1. Relation between particle size and photocatalytic activity

Kominami et al. [32] reported that the photocatalytic activity of anatase TiO_2 nanocrystals for the oxidative decomposition of acetic acid was almost proportional to the specific surface area (i.e. the amount of adsorbed acetic acid). Therefore, fine particles with large specific surface area exhibited high activity. In contrast, the photocatalytic activity for Ag^0 deposition by water oxidation depended on the crystallinity [32]. The photocatalytic activity for water oxidation is reportedly high, for well-crystallized rutile TiO_2 with large particle sizes [22–24]. The activity of TiO_2 powders is reportedly

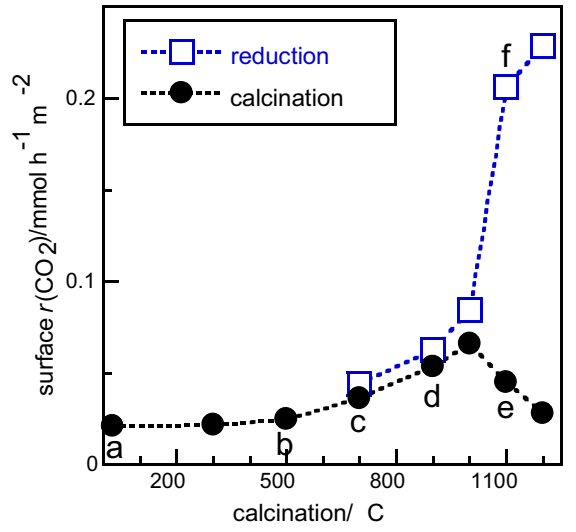

Fig. 7. $r(CO_2)$ by oxidative decomposition of acetic acid per unit of surface area over F-1R samples treated by (circles) calcination at different temperatures, and (squares) subsequent reduction with H_2 at 700 °C. Samples (a–f) are the same as those in Fig. 1.

inversely proportional to the density of surface hydroxyl groups (OH^-) and defect sites (Ti^{3+}) [22,24]. In a transient infrared spectroscopy study, the low photocatalytic activity for water oxidation by fine particulate WO_3 was attributed to the fast recombination occurring on the surface [25]. Long-lived photogenerated holes are necessary to induce the four-electron water oxidation to evolve O_2 [33,34]. Thus, large particles with low defect densities acting as recombination centers are suitable for photocatalytic O_2 evolution.

4.2. Effect of high-temperature calcination and H_2 reduction

The enhanced photocatalytic activity by H_2 reduction treatment was not due to a change in crystal structure or particle size. The diffuse reflectance spectra suggest that the incremental change in visible–NIR absorption from the increased conduction band electron concentration was related to the enhanced photocatalytic activity. Fig. 8 shows the proposed mechanism of the enhanced photocatalytic activity. Crystal growth occurred at high temperatures, and reduced the density of surface and bulk defects acting as recombination sites. This should result in the increased photocatalytic activity for water oxidation to evolve O_2. However, high temperature calcination decreased the lifetime of photogenerated electrons in TiO_2 at the same time [21]. To overcome this, O vacancies were created to donate electrons in conduction band. This improved the electrical conductivity of n-type TiO_2 particles. Improved electrical conductivity facilitated charge carrier diffusion from the bulk to the surface. The fast charge diffusion enhanced the surface charge transfer reaction. This is one of the proposed mechanisms for the enhanced surface reactivity, upon high-temperature calcination and subsequent H_2 reduction.

4.3. Particle size dependence of hydrogenation effect

The effect of H_2 reduction treatment was obtained only if the rutile particle was previously calcined at temperatures higher than 1000 °C. The calcination temperature dependence can be explained in terms of relation between the particle size of TiO_2 and the thickness of space charge layer.

An increase in the electron concentration of n-type semiconductors results in an upward shift of the Fermi level toward the conduction band edge, and the formation of a space charge region [35,36]. When n-type TiO_2 contacts with water, electron depletion layer forms at the interface, with a simultaneous potential drop (band bending) inside TiO_2. The intrinsic electric field in the space charge region separates photoexcited electrons and holes, preventing their recombination. This facilitates the transfer of holes from the valence band of TiO_2 to the reactants.

The width of space charge layer, W is determined by the donor density, N_D, and the potential drop in the layer, $\Delta\varphi_0$.

$$W = \sqrt{\frac{2\varepsilon_0\varepsilon\Delta\varphi_0}{eN_D}}$$

where ε_0 is the permittivity of vacuum, ε is the dielectric constant of semiconductor, e is electronic charge [36,37]. Assuming $\Delta\varphi_0 = 500$ mV, and taking ε for rutile to be 86, W can be calculated to be 220 nm at $N_D = 10^{17}$ cm^{-3}. The radius of particle should be larger than this thickness to obtain a band bending. Thus, high-temperature calcination is necessary to increase the TiO_2 particle size to an optimum value, ~1 μm, for space charge layer thickness.

The electron concentration equals the donor concentration for shallow donors. As the electron concentration increases, the space charge layer narrows. For example, W can be calculated to be 69 nm at $N_D = 10^{18}$ cm^{-3}. Thus, there exists an optimum electron concentration, and an optimum particle size depending on this concentration.

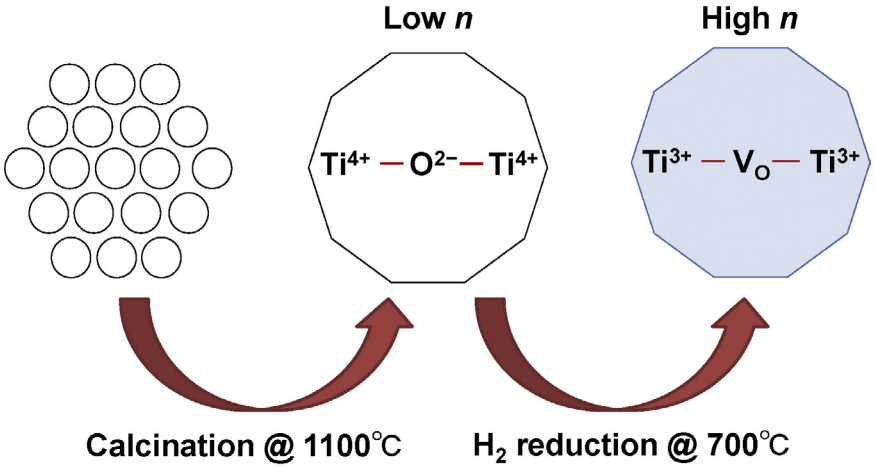

Fig. 8. Schematic showing growth of TiO_2 particles upon high-temperature calcination, and the improved surface reactivity upon H_2 treatment (*n*: electron concentration).

$$V_O + H_2O + O_O^{2-} \rightarrow 2OH^-$$

Scheme 2. Water dissociation on TiO_2 with O vacancies.

4.4. Location of O vacancy

The site of O vacancies after H_2 reduction treatment would be located in near surface region. After exposure to air at room temperature, O vacancies would play a role of active surface site for the dissociation of water molecules. Water adsorbs dissociatively in O vacancies on rutile TiO_2(1 1 0) and via H^+ transfer to a neighboring O atom creates two hydroxyl groups per initial vacancies [31]. According to Scheme 2, conduction band electron and Ti^{3+} are not associated with this water dissociation. Therefore, the hydrogenated rutile TiO_2 is stable during photocatalytic reaction in an aqueous solution.

Another possibility is that O vacancies are present exclusively in the bulk as reported in black anatase TiO_2 [38]. It is proposed that the surface disordered layer preserve the bulk phase from oxidation upon exposure to air at room temperature.

5. Conclusion

The crystalline size and O vacancy density of particulate rutile TiO_2 was controlled by high-temperature calcination and subsequent H_2 reduction. Highly efficient TiO_2 photocatalysts for water oxidation was prepared by calcination at 1100 °C and subsequent H_2 reduction at 700 °C. The hydrogenated rutile TiO_2 was stable in air at room temperature, and it was possible to use the photocatalysts repetitively. Although high-temperature calcination of particulate TiO_2 slightly improved the photocatalytic reactivity per unit of surface area, subsequent H_2 reduction is necessary to enhance the surface reactivity significantly. The enhanced reactivity was attributed to an increased electron concentration upon H_2 reduction which created oxygen vacancies. The increase of electron concentration provides improvement of n-type semiconductivity such as increase of electrical conductivity and narrowing in space charge layer. Calcination temperature dependence in the hydrogenation effect indicates that the particle size should be larger than the thickness of space charge layer. Based on this consideration, the space charge layer formed in the large crystalline particles is suggested to be involved in the activation mechanism of hydrogenated rutile TiO_2.

Acknowledgements

This work was financially supported by Japan Society for the Promotion of Science, Grants-in-Aid for Scientific Research (KAKENHI), Grant Nos. 23655187 and 23686114, and the General Sekiyu Research Scholarship Foundation. The analysis of the samples was partly carried out at the Instrumentation Center, The University of Kitakyushu.

Appendix A. Supplementary data

Supplementary material related to this article can be found, in the online version, at http://dx.doi.org/10.1016/j.apcatb.2014.04.025.

References

[1] A. Kudo, Y. Miseki, Chem. Soc. Rev. 38 (2009) 253–278.
[2] R. Abe, J. Photochem. Photobiol. C 11 (2010) 179–209.
[3] W.J. Youngblood, S.H. Anna Lee, K. Maeda, T.E. Mallouk, Acc. Chem. Res. 42 (2009) 1966–1973.
[4] M.S. Prévot, K. Sivula, J. Phys. Chem. C 117 (2013) 17879–17893.
[5] K. Maeda, ACS Catal. 3 (2013) 1486–1503.
[6] K. Maeda, Chem. Commun. 49 (2013) 8404–8406.
[7] M.K. Nowotny, L.R. Sheppard, T. Bak, J. Nowotny, J. Phys. Chem. C 112 (2008) 5275–5300.
[8] M.K. Nowotny, T. Bak, J. Nowotny, J. Phys. Chem. B 110 (2006) 16270–16282.
[9] X. Pan, M.Q. Yang, X. Fu, N. Zhang, Y.J. Xu, Nanoscale 5 (2013) 3601–3614.
[10] T. Sakata, K. Hashimoto, T. Kawai, J. Phys. Chem. 88 (1984) 5214–5221.
[11] Y. Nakato, A. Tsumura, H. Tsubomura, J. Phys. Chem. 87 (1983) 2402–2405.
[12] A. Tsujiko, T. Kisumi, Y. Magari, K. Murakoshi, Y. Nakato, J. Phys. Chem. B 104 (2000) 4873–4879.
[13] X. Chen, L. Liu, P.Y. Yu, S.S. Mao, Science 331 (2011) 746–750.
[14] G. Wang, H. Wang, Y. Ling, Y. Tang, X. Yang, R.C. Fitzmorris, C. Wang, J.Z. Zhang, Y. Li, Nano Lett. 11 (2011) 3026–3033.
[15] S. Hoang, S.P. Berglund, N.T. Hahn, A.J. Bard, C.B. Mullins, J. Am. Chem. Soc. 134 (2012) 3659–3662.
[16] G. Wang, Y. Ling, Y. Li, Nanoscale 4 (2012) 6682–6691.
[17] X. Jiang, Y. Zhang, J. Jiang, Y. Rong, Y. Wang, Y. Wu, C. Pan, J. Phys. Chem. C 116 (2012) 22619–22624.
[18] Y.H. Hu, Angew. Chem., Int. Ed. 51 (2012) 12410–12412.
[19] T. Leshuk, R. Parviz, P. Everett, H. Krishnakumar, R.A. Varin, F. Gu, ACS Appl. Mater. Interfaces 5 (2013) 1892–1895.
[20] A. Danon, K. Bhattacharyya, B.K. Vijayan, J. Lu, D.J. Sauter, K.A. Gray, P.C. Stair, E. Weitz, ACS Catal. 2 (2012) 45–49.
[21] F. Amano, M. Nakata, K. Asami, A. Yamakata, Chem. Phys. Lett. 579 (2013) 111–113.
[22] Y. Oosawa, M. Grätzel, J. Chem. Soc. Faraday Trans. 84 (1988) 197–205.
[23] T. Ohno, K. Sarukawa, M. Matsumura, J. Phys. Chem. B 105 (2001) 2417–2420.
[24] S. Ikeda, N. Sugiyama, S.Y. Murakami, H. Kominami, Y. Kera, H. Noguchi, K. Uosaki, T. Torimoto, B. Ohtani, Phys. Chem. Chem. Phys. 5 (2003) 778–783.
[25] F. Amano, E. Ishinaga, A. Yamakata, J. Phys. Chem. C 117 (2013) 22584–22590.
[26] R.A. Spurr, H. Myers, Anal. Chem. 29 (1957) 760–762.
[27] T.R. Gordon, M. Cargnello, T. Paik, F. Mangolini, R.T. Weber, P. Fornasiero, C.B. Murray, J. Am. Chem. Soc. 134 (2012) 6751–6761.

[28] Y. Miseki, H. Kusama, H. Sugihara, K. Sayama, Chem. Lett. 39 (2010) 846–847.
[29] Y. Miseki, H. Kusama, H. Sugihara, K. Sayama, J. Phys. Chem. Lett. 1 (2010) 1196–1200.
[30] K. Maeda, H. Hashiguchi, H. Masuda, R. Abe, K. Domen, J. Phys. Chem. C 112 (2008) 3447–3452.
[31] R. Schaub, P. Thostrup, N. Lopez, E. Lagsgaard, I. Stensgaard, J.K. Nurskov, F. Besenbacher, Phys. Rev. Lett. 87 (2001) 266104.
[32] H. Kominami, S.Y. Murakami, J.I. Kato, Y. Kera, B. Ohtani, J. Phys. Chem. B 106 (2002) 10501–10507.
[33] J. Tang, J.R. Durrant, D.R. Klug, J. Am. Chem. Soc. 130 (2008) 13885–13891.
[34] A.J. Cowan, C.J. Barnett, S.R. Pendlebury, M. Barroso, K. Sivula, M. Graetzel, J.R. Durrant, D.R. Klug, J. Am. Chem. Soc. 133 (2011) 10134–10140.
[35] K.E. Karakitsou, X.E. Verykios, J. Phys. Chem. 97 (1993) 1184–1189.
[36] K. Rajeshwar, in: S. Licht (Ed.), Encyclopedia of Electrochemistry, Wiley-VCH, Weinheim, 2002, pp. 1–53.
[37] A. Hagfeld, M. Grätzel, Chem. Rev. 95 (1995) 49–68.
[38] A. Naldoni, M. Allieta, S. Santangelo, M. Marelli, F. Fabbri, S. Cappelli, C.L. Bianchi, R. Psaro, V. Dal Santo, J. Am. Chem. Soc. 134 (2012) 7600–7603.